Supporting Information

A universal cross-linking binding polymer composite for ultrahigh-loading Li-ion battery electrodes

Dong Wang,[ac‡] Qian Zhang,[ac‡] Jie Liu,*[ab] Erying Zhao,[d] Zhenwei Li,[ac] Yu Yang,[ac] Ziyang Guo,[ac] Lei Wang*[ac] and Shanqing Zhang[e]

[a]Taishan Scholar Advantage and Characteristic Discipline Team of Eco-chemical Process and Technology, State Key Laboratory Base of Eco-chemical Engineering, Qingdao University of Science and Technology, Qingdao 266042, China
E-mail: jie.liu@qust.edu.cn (J. Liu), inorchemwl@126.com (L. Wang)
[b]College of Chemical Engineering, Qingdao University of Science and Technology, Qingdao 266042, China
[c]College of Chemistry and Molecular Engineering, Qingdao University of Science and Technology, Qingdao 266042, China
[d]School of Polymer Science and Engineering, Qingdao University of Science and Technology, Qingdao 266042, China
[e]Centre for Clean Environment and Energy, Environmental Futures Research Institute, School of Environment and Science, Griffith University, QLD 4222, Australia
‡These authors contributed equally.

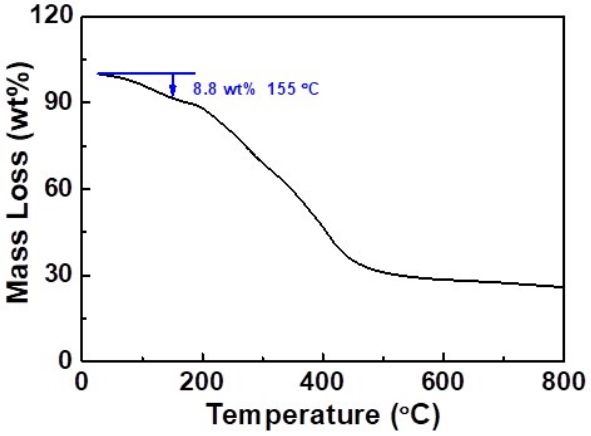

Fig. S1 TGA curve of m-PAA-XG under N_2 flow with a heating rate of 10 ℃ min^{-1}.

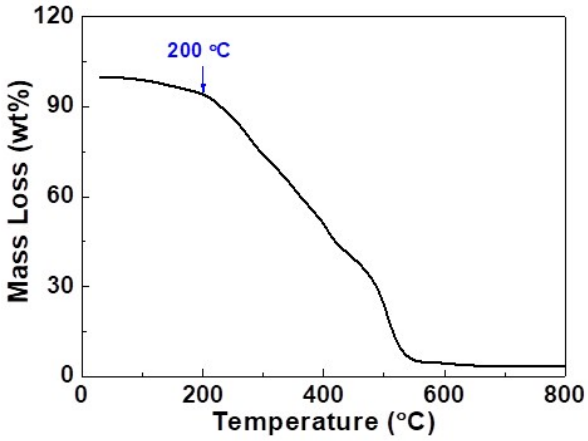

Fig. S2 TGA curve of c-PAA-XG under air flow with a heating rate of 10 ℃ min^{-1}, showing the high thermal stability (up to 200 ℃) of c-PAA-XG under air condition.

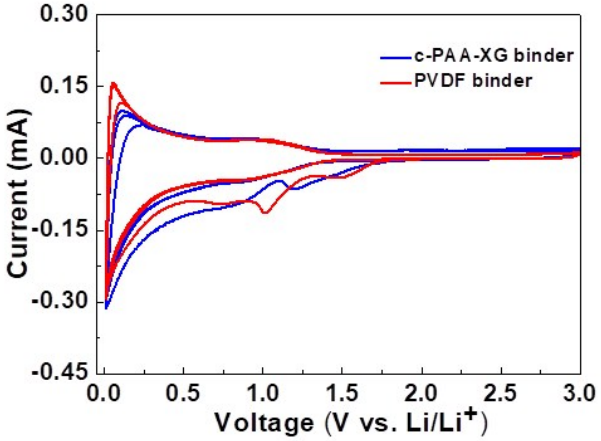

Fig. S3 Similar CV curves of PVDF and c-PAA-XG binders at 0.2 mV s^{-1}, showing the high electrochemical stability of c-PAA-XG binder. The electrodes consist of binders and super P conductive carbon with a mass ratio of 1:1.

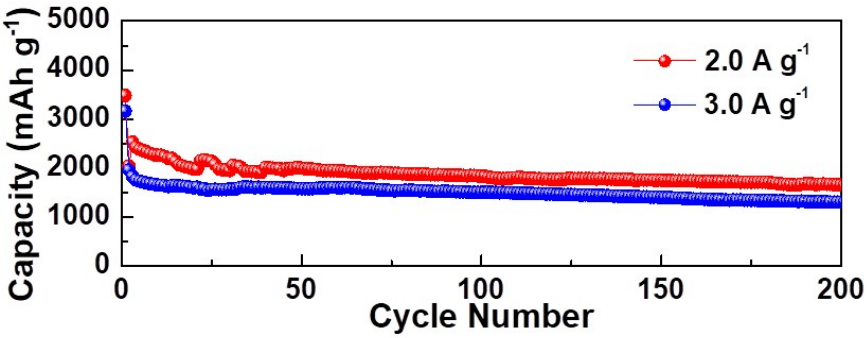

Fig. S4 Stable cycling performance of nano-Si electrodes with c-PAA-XG binders at 2.0 and 3.0 A g^{-1} (the first cycle was at 400 mA g^{-1}).

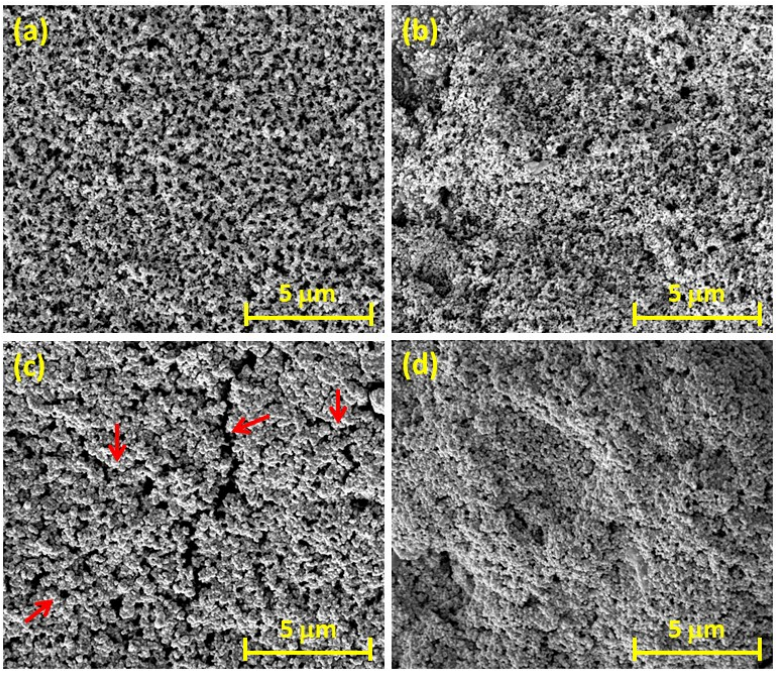

Fig. S5 SEM images of nano-Si electrodes with PVDF binder (a) before cycling and (c) after the first charge and discharge processes, and with c-PAA-XG binder (b) before cycling and (d) after the first charge and discharge processes.

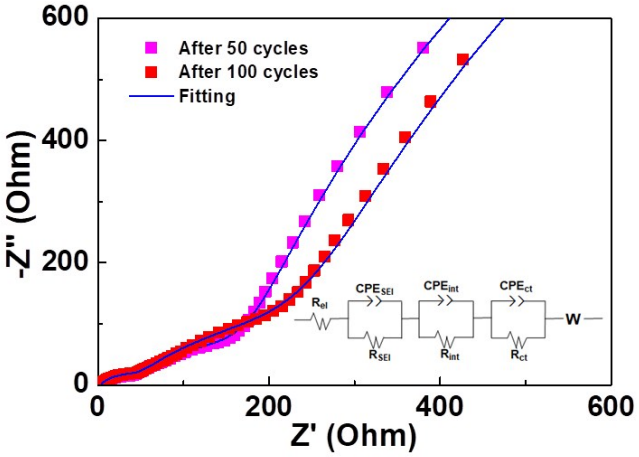

Fig. S6 Nyquist plots of nano-Si electrode with c-PAA-XG binder after 50 cycles and after 100 cycles. Inset is the fitting equivalent circuit, in which R_{SEI} is assigned to SEI film resistance, R_{int} is assigned to interphase electronic contact resistance, and R_{ct} is assigned to charge transfer resistance.

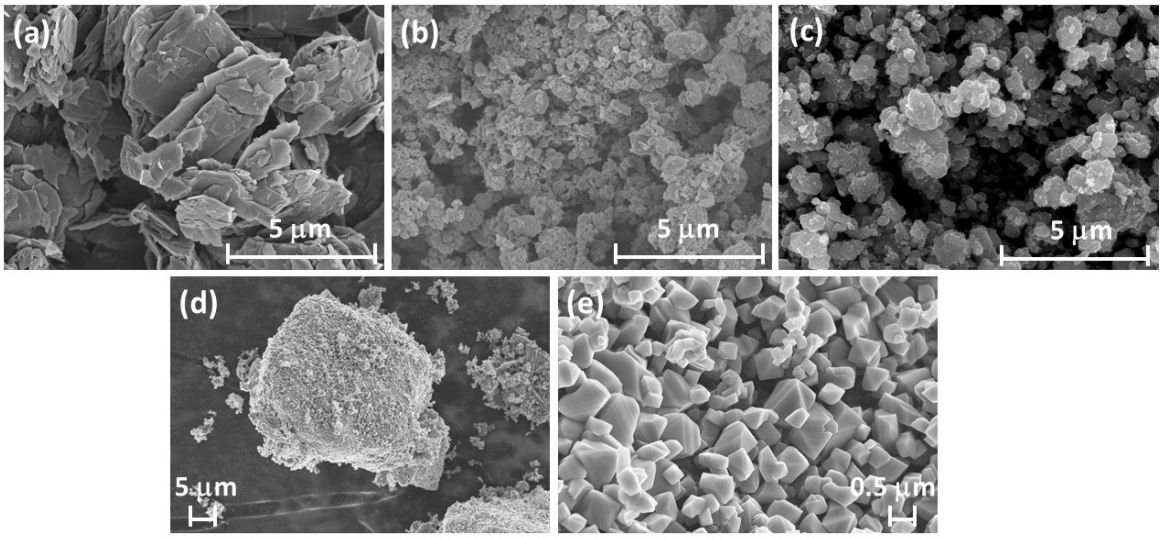

Fig. S7 SEM images of (a) graphite micro-flakes, two kinds of $LiFePO_4$ nano-particles: (b) $LiFePO_4$-1 and (c) $LiFePO_4$-2, and (d, e) $LiMn_2O_4$ nano/micro-particles.

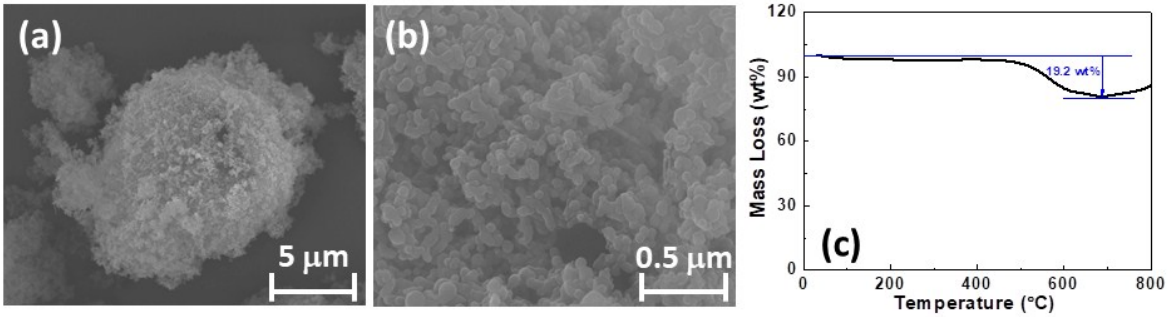

Fig. S8 (a, b) SEM images, and (c) TGA curve with a heating rate of 10 ℃ min^{-1} under air flow of as-prepared nano/micro-Si/C composite.

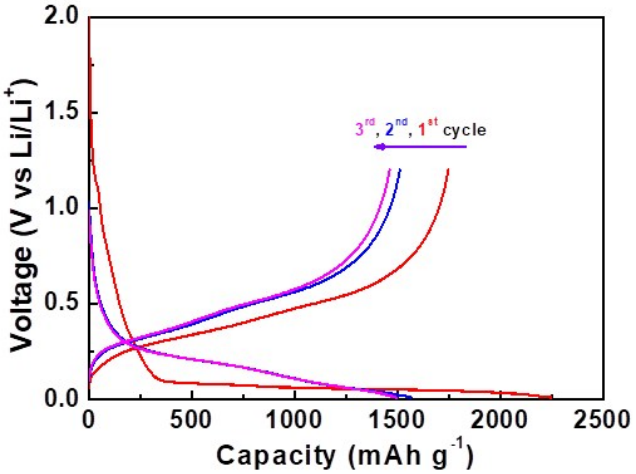

Fig. S9 Charge-discharge curves of Si/C anode with a high loading of 7.1 mg cm^{-2}.

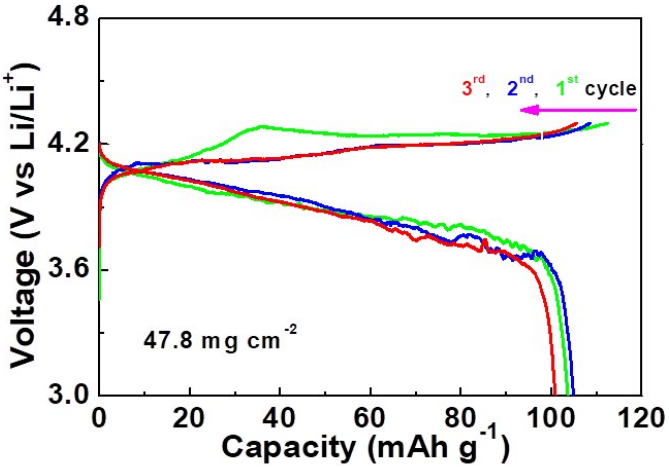

Fig. S10 Charge-discharge curves of $LiMn_2O_4$ cathode with a loading of 47.8 mg cm^{-2} at 0.03 C.

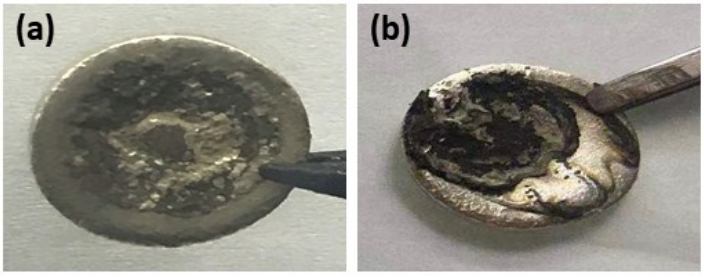

Fig. S11 Digital photos of Li anodes from the cells with: (a) graphite anode with a loading of 27.4 mg cm^{-2} after the 25^{th} charging process, and (b) $LiFePO_4$ cathode with a loading of 37.8 mg cm^{-2} after the 22^{nd} charging process.

Table S1 Comparison of the active material loading and areal capacity of Si-based anodes for Li-ion batteries in recently published excellent studies.

Ref.[a]	Active material loading (mg cm^{-2})	Reversible areal capacity[b] (mAh cm^{-2})
This work	**18.3**	**27.7**
13	1.2	1.52
22	1.1	3.2
27	0.5-0.7	1.8
46	6.2	3.2
47	4.9	~8.0
48	8.2	3.4
49	8.5	4.0
50	0.6	1.5
51	1.7	~4.2
52	0.9	2.8
53	0.35-0.5	1.1
54	0.5	1.1

[a] The references are listed in the main text

[b] The highest reversible areal capacity in the references